

Stationary States in Magnetic Resonance Imaging

Wlad T. Sobol and David M. Gauntt

*Radiology Department
University of Alabama Hospitals and Clinics
University of Alabama at Birmingham
Birmingham, Alabama 35233*

Contents

I.	Introduction	193
II.	The Origins of Ghosting	194
III.	Traditional Vector Models	194
IV.	Kaiser/Hennig Formalism	195
V.	The Balanced Protocol and Interference Artifacts	197
VI.	Unbalanced Protocols	197
VII.	Canonical Stationary States	198
VIII.	Classification of MRI Protocols	199
IX.	Conclusions	202
X.	References	202

I. Introduction

In Magnetic Resonance Imaging (MRI), the voxel position within the imaged slice is encoded using two different mechanisms. First, a magnetic field gradient (MFG) is applied during the readout of the echo data. Thus, different columns of spins, positioned at different distances along the MFG have different local frequencies that are accurately sampled during the readout time. This scheme is known as frequency (or readout) encoding. The second mechanism encodes voxel positions within columns; it requires that the entire encoding sequence is repeated many times with an MFG of varying amplitude applied along the direction within the imaged slice that is orthogonal to the readout direction. This procedure is known as phase encoding. After all the data are acquired, they are subject to the 2D Fourier Transform (2DFT). The resultant complex 2D frequency spectrum forms the final image, but

only the magnitude part of it is usually presented to the viewer.

Due to the repetitive nature of the data acquisition process, stationary states of nuclear magnetization play an important role in the design and implementation of the MR imaging protocols. A detailed understanding of physical mechanisms that determine the properties of these stationary states is especially important in the design of fast imaging protocols, when a residual transverse magnetization exists at the end of the repetition cycle. This review presents a comprehensive theory of stationary states of nuclear magnetization that focuses on practical issues related to the design and implementation of MR imaging protocols. A long list of commercial MR imaging protocols, characterized by different acronyms, is greatly simplified by using a classification scheme that is based on physical principles that form the foundation of this theory.

II. The Origins of Ghosting

The details of MRI encoding mechanisms are quite complex and could be found in the existing literature (1). However, it is the repetitive nature of the data acquisition process that is a source of most problems encountered during the design of data acquisition protocols. To better understand the nature of this problem, let's ignore the frequency encoding and focus on phase encoding process only. In the standard MR imaging algorithm the signal $S(n)$ {with $n \in [0, N]$ }, created by the phase encoding process, defines the so-called k-space in the phase encoding direction. The value of N defines the number of repetitions required to acquire data of sufficient spatial resolution (1,2). In the ideal case, the Fourier Transform (FT) of $S(n)$ produces a perfect, artifact-free image of the investigated object. Assume that due to imperfections in the acquisition process this ideal signal is modulated by some error function $f(n)$. Thus, the resulting k-space data can be written as:

$$\hat{S}(n) = f(n)S(n). \quad (1)$$

If the original, perfect image, obtained by applying the FT to the data set $S(n)$ is denoted $I(n)$, then by applying the FT to the modulated k-space data one obtains the following convoluted image:

$$\hat{I}(v) = F(v)*I(v), \quad (2)$$

where $F(v)$ is an FT of the modulating function $f(n)$. Formally, the $f(n)$ behaves like a point-spread function (PSF). In standard applications the PSF describes image blurring, caused by imperfections of the imaging system. In MRI, however, $f(n)$ usually describes ghosting, as will be discussed shortly. The reason for this difference is that in MRI $f(n)$ is always periodic and discrete, since the k-space is always sampled at some discrete intervals Δ .

Consider a case when $f(n)$ has a period ρ ; this means that its FT spectrum is a series of Dirac delta functions (see Figure 1) and:

$$\hat{I}(v) = \sum_{j=-\rho/2}^{+\rho/2} F_j \delta\left(v - \frac{j}{\rho\Delta}\right) I(v) = \quad (3)$$

$$\sum_{j=-\rho/2}^{+\rho/2} F_j I\left(v - \frac{j}{\rho\Delta}\right).$$

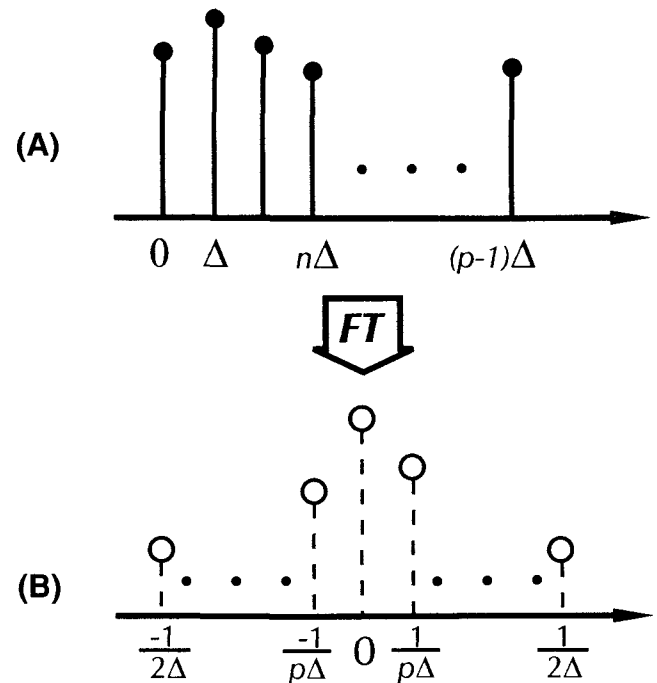


Figure 1: The behavior of the modulation function $f(n)$, generated by a stationary state of periodicity ρ (A) and its FT spectrum $F(v)$ (B). For simplicity, ρ is assumed even; the edges of the spectrum $F(v)$ correspond to the borders of the Field of View (FOV) in the regular image.

Thus, a series of ghost objects, centered at positions $j/(\rho\Delta)$, will appear in the final image. The intensity of those ghosts is determined by coefficients F_j .

Obviously, ghosts should not appear in MR images. Thus, the function $f(n)$ should have an FT spectrum containing only one component, preferably centered at zero frequency. In such a case the function $f(n)$ will be independent of n , or will contain only a DC component. In standard MRI applications this condition is ensured by using the repetition time, TR, long enough so that the spin-spin relaxation phenomena cause the residual transverse magnetization to vanish before the sequence is repeated again (with a different phase encoding MFG). In practice, this restricts the shortest TR values to about 300 ms (most tissues are characterized by a major T_2 component of about 40 - 50 ms).

III. Traditional Vector Models

The situation becomes complicated when TR is sufficiently shortened so that a residual transverse magnetization exists at the end of the cycle. Short

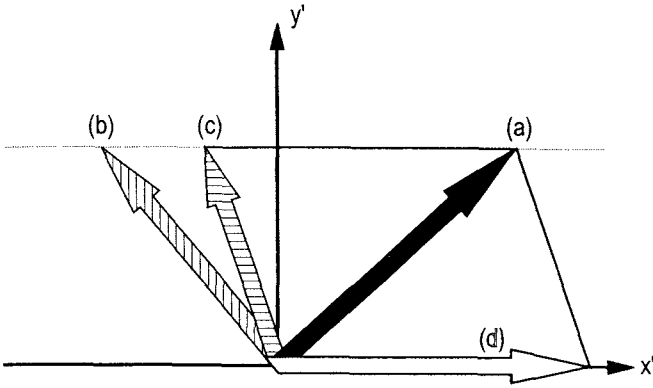


Figure 2: Vector representation of the transverse magnetization evolution within a stationary pulse cycle: (a) magnetization immediately after an rf pulse; (b) immediately before the next rf pulse - notice the precession angle from position *a* to *b*; (c) residual transverse component left in the horizontal plane by the rf pulse; (d) fresh transverse component generated by the rf pulse from the longitudinal magnetization. The vector *a* is a resultant of components *c* and *d* and thus the stationary state is restored.

TRs are desirable in practice because they reduce the exam time, often from several minutes to several seconds. Traditionally, fast MR protocol designs that produce artifact-free images are based on a vector model of a stationary state (3,4). Within this model, a stationary solution is sought for nuclear magnetization that is subject to a train of equally spaced rf pulses with equal flip angles α . It is assumed that between rf pulses the magnetization relaxes and the phase of its transverse component advances by a fixed angle φ . The motion of such a single isochromat is illustrated in Figure 2 (the rotating reference frame is used, the B_1 vector of the rf pulses is always pointing in the negative y' direction).

During the evolution period after the rf pulse, the transverse magnetization (black arrow, *a*) both shrinks in size (due to T_2 processes) and rotates around the z -axis (due to local frequency offsets). Thus, at the end of the cycle, immediately before the next rf pulse, it is found at some other position (*b*). The oncoming rf pulse shortens this component by rotating its x' projection around the y' axis (*c*). At the same time, the rf pulse rotates the longitudinal component of the magnetization, thus creating fresh horizontal projection (white arrow - *d*) that re-

stores the stationary transverse vector (black vector (*a*) is a sum of residual vector (*c*) and fresh vector (*d*)). Notice that the tips of vectors *a*, *b*, and *c* are all aligned along a single straight line, parallel to the x' axis. This happens because the rf pulse does not affect the y' components of transverse magnetization. Analytical solutions to such a stationary case have been derived (3,5,6) and successfully used in NMR spectroscopy (7,8), but they have only limited value in MRI applications. Isochromatic solutions depend on the phase advance angle φ in a complicated way. This is not a problem in NMR spectroscopy, where very uniform magnetic fields are used and phase distributions across the sample are small. In MRI, wide phase distributions are common due to the use of MFGs for slice selection and encoding of voxel positions; a single pixel value represents an NMR signal from the entire corresponding voxel. Thus, the pixel signal intensities used to create an MR image are calculated as averages over the phase distributions within the corresponding voxels:

$$\hat{S}(n) = \int_v \rho(\varphi) M(\varphi) M(\varphi, r) dV, \quad (4)$$

where $\rho(\varphi)$ is a phase distribution function normalized over the voxel's volume V and M is the transverse component of a stationary magnetization vector. Attempts to calculate these averages using solutions derived from the vector model lead to complicated equations that cannot be readily analyzed. As a result, computer models were often utilized to explore the properties of these solutions (6). Since many parameters are needed to calculate the stationary solutions (relaxation times T_1 and T_2 , spin densities, rf flip angles α , TR, phase advance φ), numerical explorations of vector solutions are tedious and costly.

IV. Kaiser/Hennig Formalism

It turns out that a formalism, first proposed by Kaiser (9) is much better suited for the studies of stationary states in MRI. Kaiser used a well known complex notation to represent transverse components of magnetization, but introduced a new way of writing a stationary solution as a Fourier series, expanded in terms of the phase advance angle:

$$M_x + iM_y \equiv F = \sum_{k=-\infty}^{+\infty} F_k e^{ik\varphi} \quad (5)$$

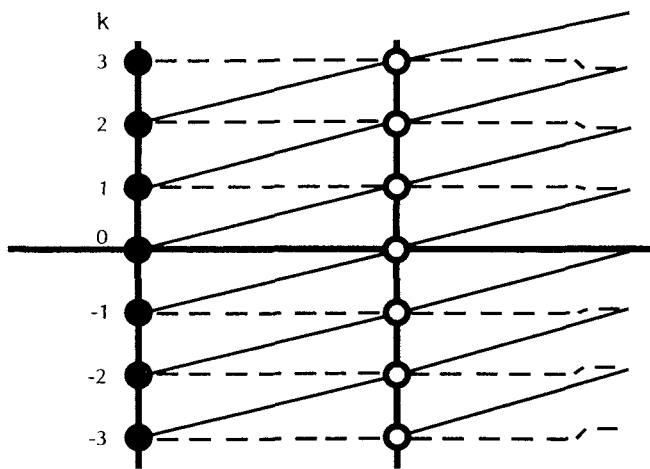


Figure 3: A Hennig phase diagram. Horizontal axis represents time, vertical axis - magnetization's phase. Vertical lines are spaced by intervals TR; nodes represent different terms of Kaiser expansion. The nodes are labelled with the Kaiser index k . Continuous lines illustrate the evolution of transverse components during the TR cycle; dashed lines represent the components of the longitudinal magnetization.

The longitudinal component of the stationary magnetization is represented in a similar fashion.

Hennig (10) has shown that this formalism can be represented graphically in a simple way by using phase diagrams. To build these diagrams, vertical lines are plotted at time intervals TR (Figure 3). A series of nodes appears on each line, representing different expansion terms in eqn. 5. Thus, the vertical axis can be viewed as a phase axis and nodes are separated by the phase advance angle φ . The transverse component precesses by an angle φ between pulses; this is schematically drawn as a solid line between nodes on two consecutive lines. The longitudinal magnetization does not acquire any phase between pulses, but "preserves" the existing phase memory among different terms of eqn. 5. This is represented by dashed lines joining the nodes. It is important to realize that the actual phase evolution between pulses does not matter, as long as the correct phase angle advancement is reached at the end of the cycle, just before the next rf pulse.

The rf pulse "mixes" different components, acting as a state generator (see Figure 4). The rf pulse generates four new components from every transverse component, entering a node: two transverse, and two longitudinal (these components are marked

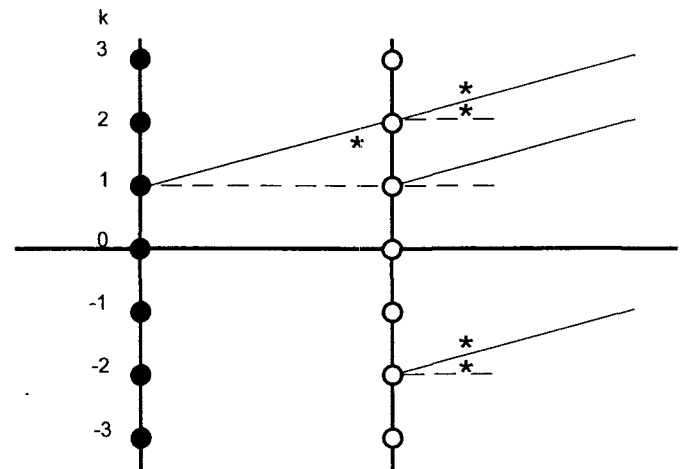


Figure 4: The effect of rf pulse as a "state generator" in the Hennig diagram. A single transverse component, marked with an *, enters the white node from the left; rf pulse at that node creates all other components, marked with an * to the right of this node line. The effect of the rf pulse on the longitudinal component is shown in a similar fashion (unmarked lines). Note the rf pulse mixes longitudinal and transverse components, as expected.

with * in Figure 4). In contrast, only two components are generated from a longitudinal trace: one transverse, one longitudinal (shown as unmarked components in Figure 4).

The entire history of magnetization evolution throughout the pulse train can be plotted using phase diagrams, constructed using the described rules. It must be noted that the value of magnetization at any given node is a superposition of contributions arising from magnetization evolution through different phase pathways, as illustrated in Figure 5. If both T_1 and T_2 were infinite, an infinite number of pathways would contribute to each node, which means that the stationary state would never be reached. Since in reality both T_1 and T_2 are finite, any perturbation of magnetization, generated by an rf pulse at any given time will eventually vanish due to relaxation phenomena. Thus, a boundary box can be created around each node: pathways outside the box do not contribute to the magnetization values at that node. The size of the box is determined by NMR characteristics of the imaged material (T_1 and T_2) as well as experimental sequence parameters (TR, α , φ). Despite this limitation, the number of paths contributing to a node can be substantial. For example, Figure 5 shows a few paths

that originate from the $k=2$ node and contribute to the $k=0$ node positioned six pulses downstream.

V. The Balanced Protocol and Interference Artifacts

Consider now a perfectly balanced MR protocol (which was introduced in the literature under a name of FISP (11) - see Figure 6). In this protocol, all MFGs used for imaging purposes are shaped in such a way that they do not contribute to the net phase gain over the repetition interval. The MFG's contribution to the phase gain is equal to:

$$\varphi'(r) = \gamma r \cdot \int_0^{TR} G(t)dt, \quad (6)$$

where γ is the gyromagnetic ratio, G represents the MFG, and r identifies a location within the imaged volume. Thus, for gradient shapes that have a zero integral over the TR interval, the net phase gain is zero anywhere within the imaged volume. For a perfectly balanced protocol the only sources of magnetization precession are local magnetic field inhomogeneities. In a large, whole-body magnet, the magnetic field varies slowly within the imaged volume. Thus, within a single voxel the phase advance angle is practically constant and the phase distribution over the voxel's volume is a Dirac's delta function, centered at a certain value φ_0 . Under such conditions, the MR signal intensity for a single voxel can be calculated from eqns. 4 and 5 and is equal to:

$$\hat{S}(n) = \int_v \delta(\varphi - \varphi_0) \sum_{k=-\infty}^{\infty} F_k e^{ik\varphi} dV = \sum_{k=-\infty}^{\infty} F_k e^{ik\varphi_0}. \quad (7)$$

Since φ_0 varies slowly across the field of view (as the magnetic field changes), for some voxels $\varphi_0=2k\pi$ and all components in eqn. 7 will add constructively, enhancing the signal intensity. There will be areas where $\varphi_0=(2k+1)\pi$ and the components will add destructively, decreasing the signal intensity. Thus, the entire image will be composed of alternating bright and dark stripes whose shape will reflect the distribution of magnetic field intensity within the FOV (12).

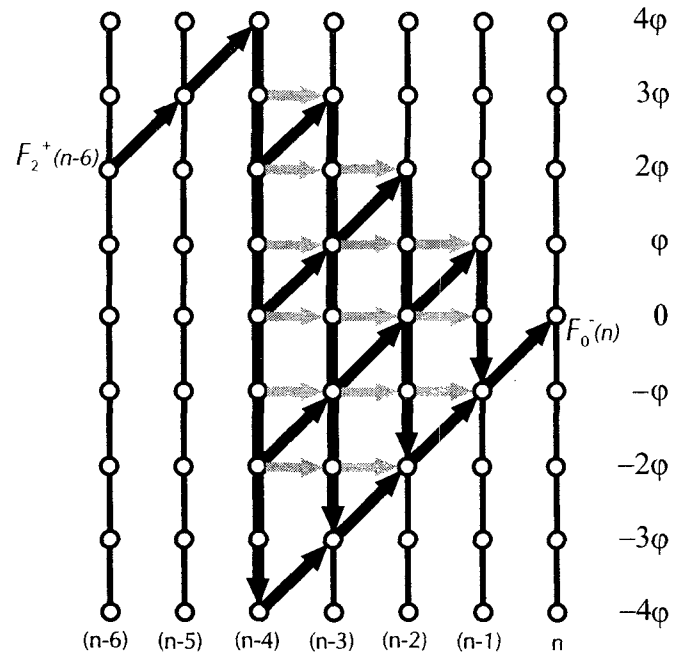


Figure 5: Coherence pathways of different magnetization components. For clarity's sake, only a few paths that originate at a node $k=+2$ and contribute to the node $k=0$ six pulses later, are shown.

The MR images created using a true FISP protocol resemble Newton rings that arise in optical interference phenomena. In fact, there is an interesting analogy between these two phenomena: both are caused by interference of many components that travel through different phase pathways and add coherently. From the practical point of view, true FISP images are useless because the interference patterns severely distort the image features that are needed for clinical diagnosis.

VI. Unbalanced Protocols

The interference problem can be solved by using unbalanced protocols. In an unbalanced protocol large phase distributions across voxels are created using the MFGs and substantial phase gains are acquired by magnetization components during the sequence cycle TR. An example of such a protocol is shown in Figure 7. The unbalanced slice select and readout gradients create a uniform phase distribution across every voxel. Let's assume that, by appropriate adjustment of the MFG shapes, the width of this distribution is forced to be a multiple

of 2π

$$\rho(\varphi) = \begin{cases} \frac{1}{2n\pi} & \text{when } -n\pi \leq \varphi \leq +n\pi \\ 0 & \text{otherwise} \end{cases} \quad (8)$$

The imaging gradients impose additional phase evolution $\phi(t)$ onto the stationary components of eqn. 5 that defines magnetization immediately following the rf pulse. Thus, at the center of data acquisition window, identified by the echo time TE, the MR signal is proportional to

$$\hat{S}(n, TE) = \int_v \rho(\varphi) \sum_{k=-\infty}^{\infty} \quad (9)$$

$$F_k e^{i(k\varphi + \phi(t)) - TE/T_2} dV = F_m e^{TE/T_2}$$

where m is an index such that

$$m\varphi + \phi(TE) = 0 \quad (10)$$

Under such conditions only one component of the entire Kaiser expansion series contributes to the signal that is acquired to produce an image. All other components, while present, are dispersed in such a way that their average value across the voxel is zero. Thus, they cannot be detected by the data acquisition method that samples the MR signals at discrete time increments Δ . The phase diagrams help to visualize this process. For the protocol shown in Figure 7, the phase path for the node $k = 0$ is shown in Figure 8. Phase paths for other remaining nodes are parallel to the path shown and are removed from the picture for the sake of clarity. It is obvious that only path for the node $k = 0$ crosses the zero phase line during the TR cycle (at a time TE). Thus, for this protocol $m = 0$ and we shall simply label such a protocol F_0 to emphasize the fact that pixel intensity values for this protocol are determined by this expansion coefficient in eqn. 5.

VII. Canonical Stationary States

The above analysis uncovers two fundamental conditions that are required to produce artifact-free images with fast MRI protocols that use short (<100 ms) repetition times TR. First, carefully designed, unbalanced gradients must be used to avoid Newton-ring type artifacts. Second, the component used to carry the image data, $F_m(n)$, must have a delta-like FT spectrum to avoid ghosts in the final

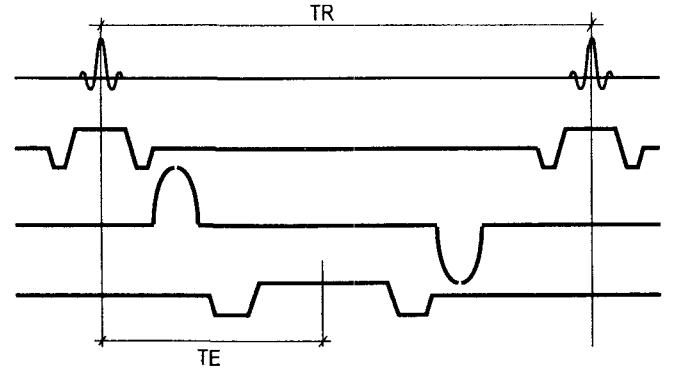


Figure 6: A balanced MR protocol. All gradients are shaped in such a way that their net contribution to the magnetization phase, integrated over the time interval TR, is zero.

image. We shall use a term *cardinal* to describe a component whose spectral delta function is positioned at the zero frequency, and label *canonical* a component that is characterized by a spectral delta function that is positioned at some nonzero offset frequency. In other words, a canonical component with zero modulation frequency is a cardinal one.

It is desirable to use cardinal components to encode the MR image data, since it is guaranteed that such an approach will produce artifact-free images without any additional data processing. If a canonical component is used to encode the MR image data, the imaged objects will be shifted off-center. This shift will be equal to the frequency offset of the spectral delta function for the canonical component used to encode the data. This offset can be calculated from the analysis of the rf sequence used, and it is a simple matter of implementing an extra processing step during the image reconstruction to shift the objects back to the center of the image.

From the above discussion it follows that it is important to identify a class of rf sequences that will produce stationary states containing only cardinal or canonical components. A detailed analysis of this problem (13) uncovered the following conditions that are necessary and sufficient to produce stationary states with canonical components:

- all rf pulses within the sequence must be equally spaced (by the time interval TR);
- all rf pulses must have the same flip angle α ;
- the phases of rf pulses δ_n ($n=0,1,2,\dots$) must satisfy the following condition (when viewed in a single rotating reference frame):

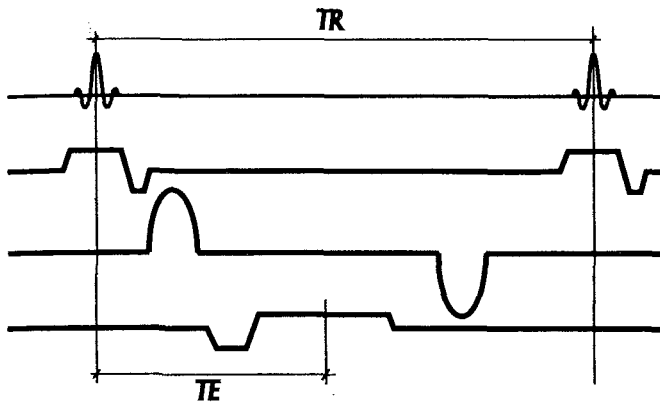


Figure 7: An unbalanced MR protocol, designed to utilize the $k=0$ node for image encoding. Note that slice select and readout gradients are unbalanced, but the phase encoding gradient remains balanced. This is because the phase encoding gradient varies among cycles.

$$\delta_n = A + Bn + Cn^2 \quad (11)$$

This result is identical to conclusions, derived by Zur et. al. (14) who analyzed ways to “spoil” transverse coherences with phase offsets of the rf pulses using Sekihara’s computer simulation method (6). To the best of our knowledge, it was Zur (15) who first proposed the use of an rf offset to effectively manipulate the stationary state. For a train of pulses with phases that follow this rule, the stationary state has a form (13):

$$F(n) = e^{i\delta_n} \sum_{k=-\infty}^{+\infty} F_k e^{iCk^2} e^{i(\varphi - B - 2Cn)k} \quad (12)$$

$$H(n) = \sum_{k=-\infty}^{+\infty} H_k e^{i(\varphi - B - 2Cn)k}$$

This equation is written in a single rotating reference frame; $F(n)$ represents transverse magnetization as defined by eqn. 5, $H(n)$ represents the longitudinal magnetization M_z . If the receiver reference phase follows the phase of the last rf pulse, then the F component in eqn. 12 must be multiplied by an exponential phase factor $(\pi/2 - \delta_n)$ and the signal is free from the transmitter phase:

$$S(n) = i \sum_{k=-\infty}^{+\infty} F_k e^{iCk^2} e^{i(\varphi - B - 2Cn)k}. \quad (13)$$

From eqn. 13 it follows that the value of A will not affect the stationary state conditions. This is to

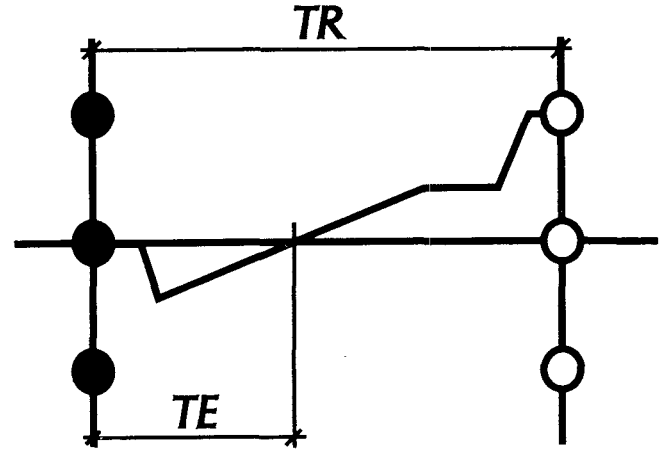


Figure 8: Phase path for the node $k=0$ for the MR protocol shown in Figure 7. Phase paths for other nodes are parallel to the one shown and are not visualized for simplicity.

be expected, as A represents a constant phase offset. The value of B describes a frequency offset between the rf carrier frequency and the reference frequency of the rotating frame. Under normal imaging conditions when unbalanced gradients are used, the value of B does not affect the image contrast, because it simply offsets the center of the distribution function $\rho(\varphi)$ by B (see eqn. 8). This shift, however, will affect the distribution of the interferences stripes created with a balanced protocol (see eqn. 7). An imaging scheme that takes advantage of this phenomenon to create true FISP images has been proposed under the name CISS (16). The selection of coefficient C will definitely affect the stationary state. Thus, we shall denote by $F_m(C)$ the protocol that uses an m -th node of the stationary state created with a train of rf pulses determined by the value of constant C .

VIII. Classification of MRI Protocols

Using the presented arguments one can classify the existing MR imaging protocols into categories, according to tissue contrast they produce. Both m and C do affect the image contrast, thus all protocols that use $F_m(C)$ component of the Kaiser expansion to encode image data will produce images that are equivalent in terms of image contrast, regardless of details of the protocol implementation. This is an important feature since it allows one to simplify the long list of acronyms that MR equip-

Table 1: Commercial equivalents of $F_0(0)$ protocol.

Full Name	Acronym	Manufacturer
Fourier Acquired Steady State	FAST	Picker International
Field Echo	FE	Toshiba America MS
Fast Field Echo	FFE	Philips MS
Fast Field Echo	FFE	Otsuka Electronics
Fast Imaging with Steady State Precision	FISP	Siemens MS
FID-based short repetition technique	F-SHORT	Elscont
Gradient Field Echo with Contrast	GFEC	Hitachi MS America
Gradient Recalled Acquisition in the Steady State	GRASS	GE MS
Steady State Free Precession	SSFP	Shimadzu MS

Note: MS = Medical Systems. Entries are listed in alphabetical order of acronyms.

ment vendors introduced in recent years to describe the imaging capabilities of their hardware. Different hardware platforms and different developmental paths lead to different, proprietary implementation strategies that were described using different acronyms. However, all protocols must function using the same physics principles and thus, when implemented correctly, will produce equivalent results despite hardware-related differences in implementation details.

The protocols with $C=0$ are easiest to implement, and two are widely used. The first one, $F_0(0)$ is simply an implementation of the method that uses the $m=0$ node, as illustrated in Figure 7 and Figure 8. This is the most intuitive, and thus most widely used protocol. The commercial equivalents of this protocol are listed in Table 1. Another $C=0$ protocol is shown in Figure 9. The analysis of phase evolution using the phase diagrams immediately identifies this protocol as $F_{-1}(0)$, as seen in Figure 10 (the commercial equivalents of this protocol are listed in Table 2).

At this stage, the advantages of using Fourier expansion technique with phase diagrams become very clear. Methods that use traditional vector models identify the $F_0(0)$ protocol as FID, due to its obvious association with the signal that is implicitly generated by the rf pulse. Similarly, the $F_{-1}(0)$ protocol is identified as an “echo” protocol, since it appears to sample a spin echo signal (the spin echoes were first described by Hahn who analyzed a series of three arbitrary rf pulses (17)). It is quite obvious

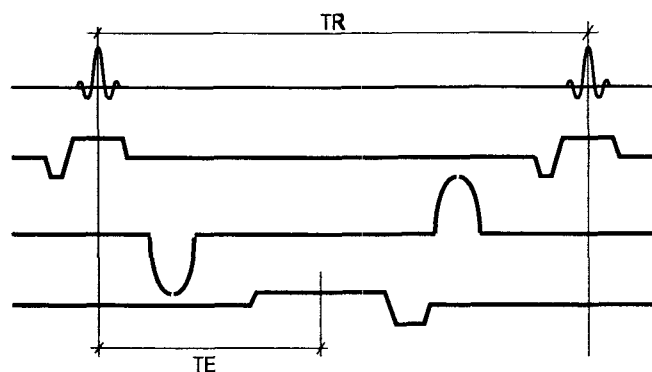


Figure 9: An F_{-1} MR protocol.

from Figure 5 that such association is misleading, since both signals actually represent superpositions of many components (that were originally identified by Hahn as sources of separate echoes). From the phase diagrams it is also quite obvious that either signal can be used to create an MR “echo” anywhere within the TR interval by using appropriately shaped MFGs (see Figure 8 and Figure 9). If the MFGs are properly designed, no mixing of the two signals will occur. Furthermore, the vector model describes only two different types of images, associated with either FID or echo signals. It is obvious from the phase diagrams that, in principle, an infinite number of different images can be created by using different nodes to encode image data. For example, Figure 11 shows a protocol that encodes the $m=+1$ node (see Figure 12). Nobody has used such a protocol in practice yet, probably because people were unaware of the fact that it could be done.

For the Kaiser expansion to be convergent, the values of expansion coefficients F_k must decrease

Table 2: Commercial equivalents of $F_{-1}(0)$ protocol.

Full Name	Acronym	Manufacturer
Contrast Enhanced Fourier Acquired Steady State	CE-FAST	Picker International
Contrast Enhanced Fast Field Echo with T_2 weighting	CE-FFE- T_2 , T_2 -FFE	Philips MS
Echo-based short repetition technique	E-SHORT	Elscent
Reversed FISP	PSIF	Siemens MS
Steady State Free Precession	SSFP	GE MS
Steady State Technique with Refocused FID	STERF	Shimadzu MS

Note: MS = Medical Systems. Entries are listed in alphabetical order of acronyms.

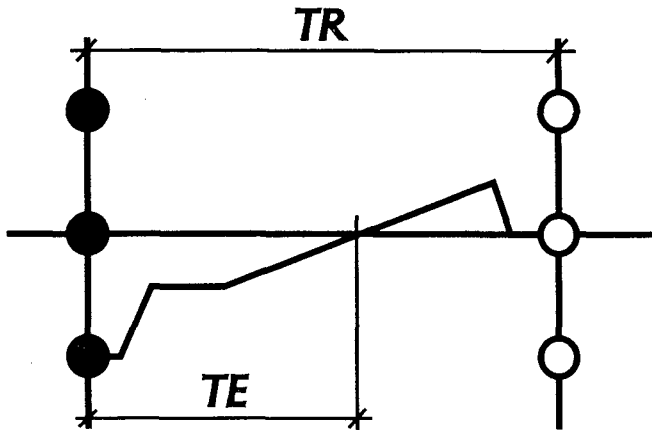


Figure 10: The phase path for node $k = -1$ for the MR protocol shown in Figure 9. Note: the definition of the echo time TE for this protocol varies among different sources and may not correspond to the value indicated.

quickly with increasing k . This leads to rapid signal-to-noise deterioration when higher order nodes are selected to encode the image data. This signal-to-noise deterioration, as well as the need to use very large gradients to encode higher order nodes makes their use impractical today. But the possibilities exist and might be used someday in MRI practice.

The literature describing protocols that use nonzero C values is often confusing, chiefly because the vector models do not support such concepts very well. It is generally stipulated that such protocols lead to "magnetization spoiling" that prevents transverse components from contributing to the stationary state and thus the resulting image contrast does not depend on T_2 anymore. Existing numerical simulations (14) and recent analytical analysis (13) of these protocols indicate that this is not the case. Image contrast between two different tissues (characterized by different spin densities, T_{1s} and T_{2s})

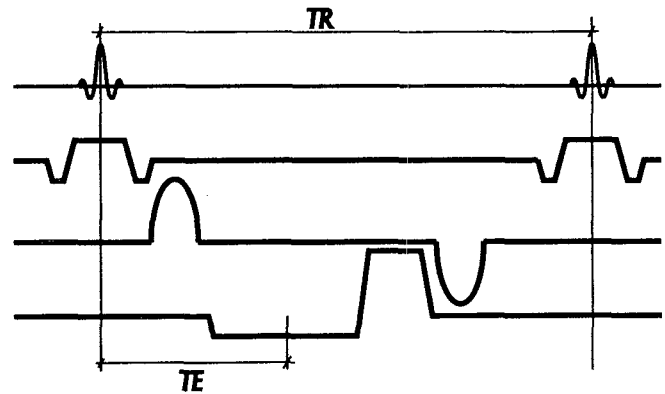


Figure 11: An F_{+1} MR protocol.

strongly depends upon the values of C and can be extensively manipulated. It usually exhibits a resonant behavior, with resonances of various strength occurring for specific values of C that create periodic cycles within the sequence train (13). Thus, a continuum of image contrasts is available and an important question arises how to select the values of parameter C to ensure optimal image contrast in clinical applications of these protocols. This issue is not resolved yet, but it has been significantly facilitated by recent presentation of analytical solutions for resonant values of C (13).

An efficient way to implement the spoiled protocols requires digital rf hardware to precisely control the phases of rf pulses. In such a case, the basic imaging sequence follows the normal scheme (see Figures 7, 9, 11), but the phases of rf pulses are varied according to eqn. 11. An example of such a solution is a commercial SPGR protocol (GE Medical Systems, Milwaukee, WI) that uses $C = 46.184^\circ$. For systems for which the digital hardware is not yet available, various gradient spoiling techniques have been proposed to achieve equivalent results.

Table 3: Commercial equivalents of $F_0(0)$ protocol.

Full Name	Acronym	Manufacturer
Contrast Enhanced Fast Field Echo with T_1 weighting	CE-FFE- T_1 , T_1 -FFE	Philips MS
Fast Low Angle Shot	FLASH	Siemens MS
Partial Saturation	PS	Instrumentarium Imaging
RF spoiled FAST	RF-FAST, T_1 -FAST	Picker International
Short repetition technique	SHORT	Elscint
Spoiled GRASS	SPGR	GE MS
Small Tip Angle Gradient Echo	STAGE	Shimadzu MS

Note: MS = Medical Systems. Entries are listed in alphabetical order of acronyms.

It is much more difficult to avoid image artifacts when using MFGs to create the required phase offsets within the TR cycles. The difficulties arise from the fact that MFG used in MR imaging protocols must often be scaled to allow changes in slice thicknesses, the size of the field of view, or the data acquisition bandwidth (often related to the TE used). The gradient spoiling scheme must produce phase advancements that are independent of the above parameters.

To date, all commercial applications utilize the $F_0(C)$ protocol (see Table 3). Again, this is probably due to the fact that vector models failed to indicate that other options are possible. However, for $C \neq 0$ the $m \neq 0$ components are not cardinal, but canonical (see eqn. 13). If C is known, the required frequency shift can be easily calculated, but additional image processing step is required to correct it. It remains to be seen if more complex applications, based on $F_m(C)$ protocols find their way into clinical practice.

IX. Conclusions

The Kaiser expansion method, combined with the Hennig phase diagrams provide a powerful tool to investigate stationary magnetization states useful in generation of artifact-free MR images. Such an approach opens a way to classify different MR protocols according to their underlying physical principles. In addition to existing commercial protocols that all fit into this classification scheme, new ones, so far not implemented in practice, are discovered. Analytical solutions for stationary states responsi-

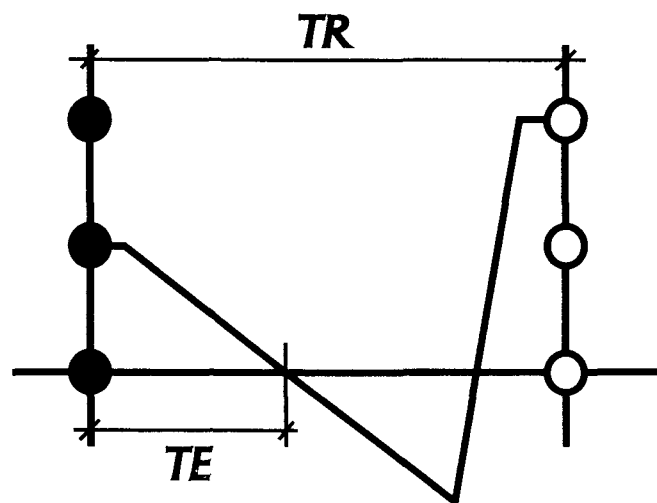


Figure 12: The phase path for node $k = +1$ for the MR protocol shown in Figure 11.

ble for tissue contrast in the resulting MR images further facilitate studies of this exciting, but quite unwieldy branch of applied NMR physics.

X. References

- ¹M. Bronskill, P. Sprawls, Eds. The Physics of MR Imaging. AAPM Monograph 21, AIP, New York, (1993).
- ²D.B. Twieg, *Med. Phys.* **10**, 610 (1983).
- ³P. van der Meulen, J.P. Groen, A.M.C. Tinus, G. Bruntink, *Magn. Reson. Imaging* **6**, 353 (1988).
- ⁴F.W. Wehrli, Fast Scan Magnetic Resonance. Principles and Applications. Raven Press, New York, (1991).
- ⁵M.L. Gyngell, *J. Magn. Reson.* **81**, 427 (1989).
- ⁶K. Sekihara, *IEEE Trans. Med. Imaging* **MI-6**,

157 (1987).

⁷W.S. Hinshaw, *J. Appl. Phys.* **47**, 3709 (1976).

⁸R. Freeman, H.D.W. Hill, *J. Magn. Reson.* **4**, 366 (1971).

⁹R. Kaiser, E. Barholdi, R.R. Ernst, *J. Chem. Phys.* **60**, 2966 (1974).

¹⁰J. Hennig, *J. Magn. Reson.* **78**, 397 (1988).

¹¹A. Oppelt, R. Graumann, H. Barfuss, H. Fisher, W. Hartl, W. Schajor, *Electromedica* **54**, 15 (1986).

¹²J. Hennig, *Concepts in Magnetic Resonance* **3**, 179 (1991).

¹³W.T. Sobol, D.M. Gauntt, On Stationary States in Gradient Echo Imaging. *J. Magn. Reson. Imag.* **6**, 384 (1996).

¹⁴Y. Zur, M.L. Wood, L.J. Neuringer, *Magn. Reson. Med.* **21**, 251 (1991).

¹⁵Y. Zur, P. Bendel, Sixth Annual Meeting of the Society of Magnetic Resonance in Medicine, New York, 1987, p.440.

¹⁶J.W. Casselman, R. Kuhweide, M. Deimling, W. Ampe, I. Dehaene, L. Meeus, *AJNR* **14**, 47 (1993).

¹⁷E.L. Hahn, *Phys. Rev.* **50**, 580 (1950).